A Versatile Integrated Circuit for the Acquisition of Biopotentials

Reid R. Harrison[1,2]

[1]Department of Electrical & Computer Engineering
University of Utah
Salt Lake City, UT 84112 USA

[2]Intan Technologies, LLC
Salt Lake City, UT 84121 USA

***Abstract*—Electrically active cells in the body produce a wide variety of voltage signals that are useful for medical diagnosis and scientific investigation. These biopotentials span a wide range of amplitudes and frequencies. We have developed a versatile front-end integrated circuit that can be used to amplify many types of bioelectrical signals. The 0.6-µm CMOS chip contains 16 fully-differential amplifiers with gains of 46 dB, $2\mu V_{rms}$ input-referred noise, and bandwidths programmable from 10Hz to 10kHz.**

I. Introduction

In all animals (and some plants [1]), information is transmitted and physical motion is initiated using both chemical and electrical signals. Most electrically active cells can modulate their internal voltage by approximately 100 mV with respect to the extracellular fluid through the use of ion channels embedded in their membranes [2]. While intracellular recordings from single cells are possible for relatively brief periods of time if careful micropositioning equipment is used, the most practical methods for long-term biopotential recording observe cells from a distance.

The most commonly observed biopotentials used in medical diagnoses can be monitored non-invasively with electrodes placed on the surface of the skin [3]. These include the electrocardiogram, or ECG (sometimes known by its German acronym as EKG), which monitors heart activity; the electromyogram (EMG) which monitors other muscle activity in the body; and the electroencephalolgram (EEG) which monitors electrical activity in the brain via weak potentials on the scalp.

Implanted microwires or MEMS electrodes can observe biopotentials such as the EMG with greater fidelity. Implanted electrodes can also be placed in the brain to permit direct recording of individual neural action potentials, or "spikes" (e.g., [4], [5]). In addition to monitoring the individual activity of a few nearby neurons, an electrode in the brain can observe low-frequency oscillations corresponding to the collective, synchronous activity of thousands of relatively distant neurons. These signals, known as local field potentials (LFPs), are the internal correlate of the EEG signals observed on the scalp (after significant attenuation and spatial blurring).

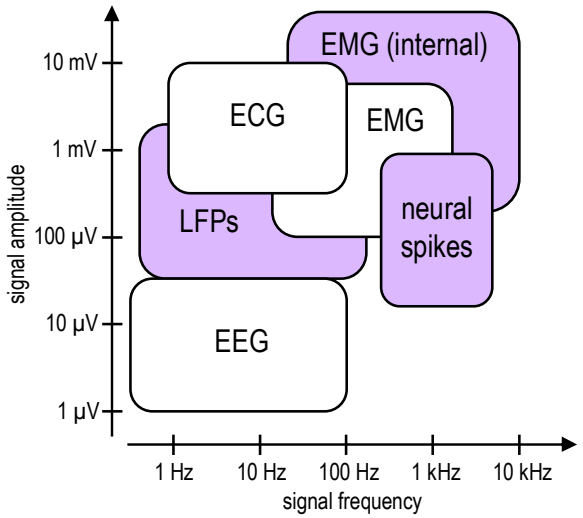

Fig. 1. Approximate frequency content and amplitude distribution of common biopotentials recorded from the surface of the skin (white boxes) or internally (shaded boxes).

Fig. 1 shows the approximate frequency content and amplitude distribution of common biopotentials of medical and scientific interest. These signals span over four decades of frequency, from less than 1 Hz to around 10 kHz, and over four decades of amplitude, from 1 µV to over 10 mV.

Traditionally, these weak electrical signals have been amplified, filtered, and conditioned using bulky rack-mounted equipment. Recent advances in packaging, assembly, and integration have led to the development of small wearable and implantable medical and scientific instruments. To advance device miniaturization, we have developed an integrated array of 16 fully-differential low-noise biopotential amplifiers with an on-chip analog multiplexer (MUX). No off-chip capacitors are required to obtain low-frequency ac-coupled amplification, and two off-chip resistors allow the user to configure the amplifier bandwidth to optimize the recording of the biopotential signals shown in Fig. 1. In Section II we describe the nature of the electrode-tissue interface, which is the source of our signals. In Section III we introduce the amplifier circuits, and in Section IV we present experimental results from the fabricated chip including benchtop characterization as well as actual biopotential signals recorded using the chip. We conclude the paper in Section V.

1-4244-1623-X/07/$25.00 ©2007 IEEE

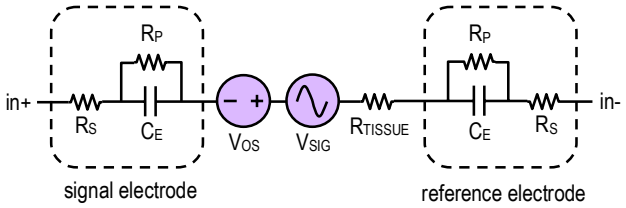

Fig. 2. Approximate small-signal model of biopotential recording site with differential measurement using a signal and reference electrode.

II. The Electrode-Tissue Interface

All biopotential recording systems require a physical interface between the metallic wires of the electronic circuits (where current is carried by electrons) and biological tissue (where current is carried by ions). For ECG and EMG applications this interface usually takes the form of Ag/AgCl electrodes approximately 1-2 cm in diameter that adhere to the surface of the skin. A thin layer of electrolyte-filled foam or gel separates the metal electrode from the skin, reducing artifacts caused by the relative movement of skin and electrode. EEG recording systems often use Ag/AgCl electrodes held close to the head with a snug-fitting cap. Electrolyte gel is injected between each electrode and the scalp to provide a stable, conductive path through the hair. It is also possible to record biopotentials from the skin using dry stainless steel electrodes, but these are more susceptible to movement artifacts.

Implanted systems such as neural or intramuscular EMG recording devices typically use platinum or platinum-iridium electrodes constructed from fine wire or MEMS structures (e.g., [4], [5]). The electrode is immersed in the extracellular fluid of the brain or muscle tissue and records the activity of nearby cells.

In all electrode-tissue interfaces, an electrical double layer forms once equilibrium is reached. For small voltage and current levels, this interface behaves primarily as a capacitance. Textbook models of electrodes often include a resistance R_P in parallel with the electrode capacitance C_E, as well as a series resistance R_S (see Fig. 2). The contact between the metallic electrode and the electrolytic solution (i.e., gel or extracellular fluid) also produces a dc offset, shown as V_{OS} in Fig. 2. The sign and magnitude of this potential are functions of material properties, tissue condition, and temperature, and are difficult to predict. Most external biopotential recording systems are designed to tolerate dc offsets of ±300 mV, and implanted electrodes can exhibit similar built-in potentials.

We model the biopotential as an ac voltage source V_{SIG} in series with a resistance R_{TISSUE} that represents the conductive tissue between the signal and reference electrodes. Although the equivalent circuit shown in Fig. 2 is a useful first-order model for low-voltage recording applications, it is important to realize that the actual electrode-tissue interface is a complex, nonlinear, time-variant structure that is difficult to model in any general or precise way. The resistance and capacitance values in this model typically vary with frequency and signal amplitude.

In external recording systems for ECG, EMG, or EEG, the signal and reference electrode are typically identical in size and structure; differential recording from two nearby points on the body is used to minimize pickup of 50/60-Hz power line interference. (The in+ and in- terminals in Fig. 2 would be connected to the input of a differential amplifier.) In addition to the differential recording electrodes, a third electrode is used to tie the body to circuit ground in order to guarantee a reasonable dc potential at the amplifier input. The site of the ground electrode is usually chosen to be a part of the body with little electrical activity present (i.e., no nearby muscles). When EMG signals are recorded from the arm, the ground electrode is often attached to the bony tip of the elbow; EEG systems usually use ground leads attached to the earlobes.

To provide an example of electrode properties in a typical biopotential recording situation, we characterized the impedance of Ag/AgCl conductive foam adhesive electrodes (Kendall-LTP, Chicopee, MA) positioned for EMG recording on the bicep approximately 5 cm apart. At 1 kHz, we measured C_E = 60 nF, R_P = 210 kΩ, R_S = 7 Ω, and R_{TISSUE} = 1.7 kΩ. Note that C_E has an impedance magnitude much smaller than R_P at this frequency, so R_P has little effect and contributes little Johnson noise to the recording.

Implantable microelectrodes have small surface areas and thus high impedances, so a low-impedance bare platinum wire a few centimeters in length is often used as a common reference electrode. By convention, the impedance of microelectrodes used for neural recording is almost always reported as the magnitude of the impedance at 1 kHz. For example, it is commonly reported in bioengineering and neuroscience literature that a "1 MΩ electrode" was used, for example. The omitted details – that this is only the *magnitude* of the impedance (which almost always has a phase angle very near –90°) measured *at 1 kHz* – misleads many people new to the field into believing that the electrode has 1 MΩ of *real* resistance due to its small size. This would indeed be an unfortunate situation for recording small neural signals since a 1-MΩ resistor generates 13 μV_{rms} of Johnson noise across a typical recording bandwidth of 10 kHz. (In modern microelectrodes, the real series resistance R_S is typically less than 10 kΩ.) Most microelectrodes used for neural recording have values of C_E ranging from 0.16 nF to 16 nF (depending on electrode surface area and surface roughness), leading to commonly-cited electrode impedance magnitudes in the range of 10 kΩ – 1 MΩ at 1 kHz. As with external electrodes, the value of R_P is usually much greater than the impedance of C_E at signal frequencies.

One consequence of the complex, ill-defined nature of the electrode-tissue interface is that it is impossible to derive the noise figure (NF) of a biopotential amplifier since the concept of noise figure was developed for systems having a well-defined source impedance (e.g., 50 Ω). Instead, biopotential amplifiers are characterized by their input-referred noise measured across their bandwidth.

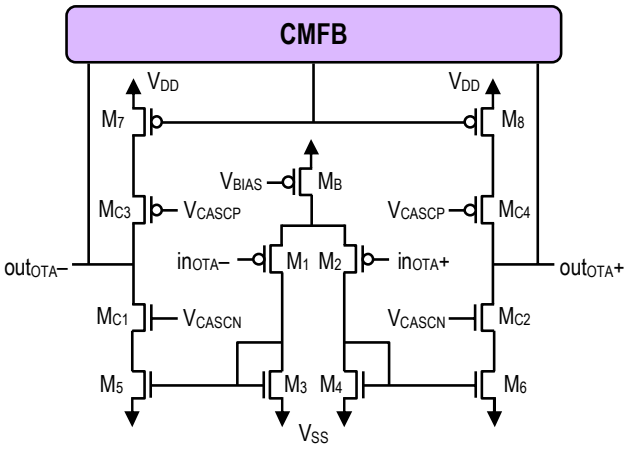

Fig. 3. Schematic of operational transconductance amplifier (OTA) used in the first stage of the biopotential amplifier.

III. Circuit Design

In previous work, we developed a design technique to minimize the noise efficiency factor (NEF) and thus optimize the power-noise trade-off in biopotential amplifier design [6]. Using drain currents (I_D) in the high nanoampere or low microampere range, CMOS transistors can be operated either in strong inversion (above threshold), moderate inversion, or weak inversion (subthreshold) by appropriate sizing of their width-to-length ratio (W/L) [7], [8]. Using a current-mirror amplifier topology, the differential pair transistors are operated in weak inversion to maximize g_m/I_D, and the current mirror transistors are operated in strong inversion to minimize g_m/I_D. In this paper we apply this method to a fully-differential two-stage CMOS amplifier with a third-order Butterworth low-pass filter response.

Fig. 3 shows a schematic of a fully-differential operational transconductance amplifier (OTA) used in the first stage of our biopotential amplifier. The transconductance G_m of the amplifier is controlled by the bias current from transistor M_B. The bias current can be varied from 20 nA to 40 μA by means of a bias generator circuit [9] that employs an off-chip resistor to select the current level and thus the OTA transconductance. The differential pair transistors M_1-M_2 are drawn wide ($W/L >$ 500) to maintain weak or moderate inversion operation. The current mirror transistors M_3-M_6, as well as M_7-M_8, are drawn narrow ($W/L < 1$) to maintain strong or moderate inversion operation. This design minimizes input-referred noise for a given bias current [6]. Cascode devices M_{C1}-M_{C4} increase the output resistance of the OTA. A common-mode feedback (CMFB) circuit maintains the dc level of the two output nodes halfway between V_{SS} and V_{DD}.

Fig. 4 shows a schematic of the two-stage amplifier. The first stage uses the fully-differential OTA from Fig. 3 in a differential amplifier configuration with capacitive feedback. The midband gain of the first stage is set by the capacitor ratio C_1/C_2, and is thus well controlled. The high-frequency bandwidth of the first stage is set by G_m and the load capacitance C_L. Thus, by varying the bias current in the OTA, the bandwidth of the first stage may be tuned.

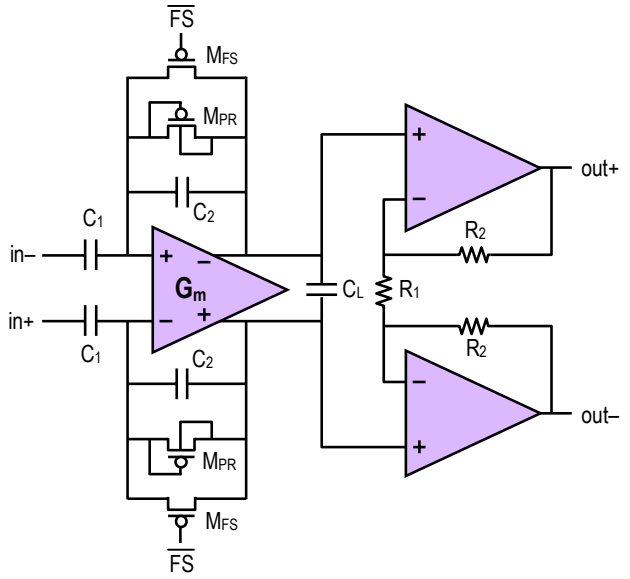

Fig. 4. Schematic of the complete two-stage biopotential amplifier.

The input capacitors (C_1) block dc electrode-tissue offset voltages. The low-frequency cutoff f_L is $1/2\pi R_{PR}C_2$, where R_{PR} is the equivalent small-signal resistance of the MOS-bipolar "pseudo-resistor" element M_{PR} [6]. Extremely high values of R_{PR} are obtained, yielding values of f_L below 0.1 Hz. While an amplifier response below 1 Hz is desirable in many biopotential recording applications (see Fig. 1), the long time constant associated with such a circuit leads to slow recovery from overloads or other large disturbances. To address this problem, we added a "fast settle" function; when the M_{FS} transistors are turned on by the digital, active-low FS signal, the amplifier output quickly returns to baseline.

The second stage is a standard instrumentation amplifier topology with resistive feedback setting the gain to $1+2R_2/R_1$. The unity-gain frequencies of the operational amplifiers in this stage are also controlled by adjustable bias currents, so their bandwidth may be programmed using a second off-chip resistor as part of a bias generator circuit. The poles in these op amps are calibrated to yield a phase margin of 52° for the closed-loop gain set by R_1 and R_2. This leads to a system having a second-order low-pass response with a quality factor $Q = 1$. By setting the characteristic frequency ω_0 of the second stage equal to the –3 dB frequency of the first stage (which has a phase margin of close to 90° and thus behaves as a first-order system), we obtain a third-order Butterworth low-pass filter with a maximally flat passband and a stopband roll-off of –60 dB/decade. By choosing appropriate values for the two off-chip resistors, we can align the cutoff frequencies to produce proper poles for a Butterworth filter.

Fig. 5 shows a block diagram of the complete 16-channel amplifier chip. An analog MUX controlled by the digital signals Select0 – Select3 allows all 16 amplifiers to share one analog-to-digital converter (not included on this chip). The MUX includes fast unity-gain buffers to allow each channel to be sampled up to 30 kS/s. Fully-differential design throughout the chip minimizes noise from common-mode interference.

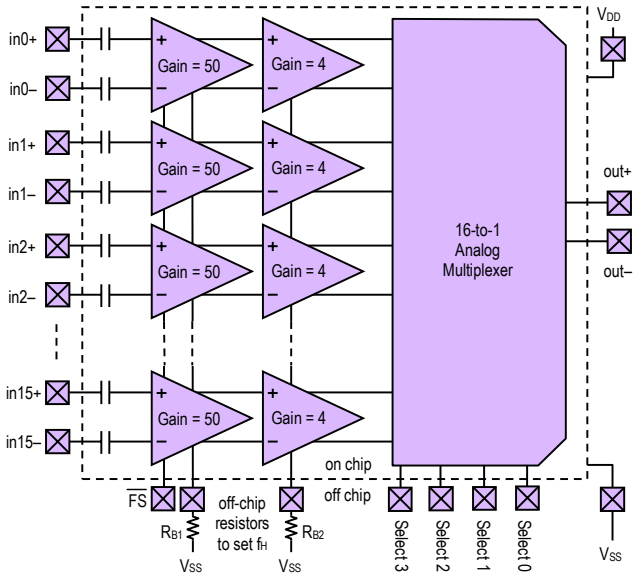

Fig. 5. Block diagram of 16-channel RHA1016 bioamplifier IC.

IV. Experimental Results

A. Benchtop Characterization

We fabricated the 16-amplifier chip (designated RHA1016) in a 0.6-µm 2M2P CMOS process with linear metal-insulator-metal (MIM) capacitors. The total silicon area used for circuitry and pads measured 4.2 × 2.8 mm^2; the diced chip measured 4.3 × 3.1 mm^2 (see Fig. 6). Each amplifier channel, including analog MUX circuitry, consumed 0.37 mm^2. The chip operates from a single +5V supply. The only off-chip components required are the two resistors used to set the high-frequency bandwidth f_H. By varying the values of these two resistors, f_H can be programmed to any frequency from 10 Hz to 10 kHz.

As shown in Fig. 5, the total gain of each two-stage amplifier was set to 200 V/V (46 dB) with appropriate capacitor and resistor ratios; this gain was confirmed by measurement. Fig. 7 shows the measured *normalized* gain (i.e., with the midband gain of 46 dB subtracted) of one amplifier with f_H set to 1 kHz. The 3rd-order Butterworth low-pass response of the amplifier is evident, with a flat passband, the –3dB drop in gain at 1 kHz, and a –60 dB drop precisely one decade higher at 10 kHz. The phase response of the same amplifier is shown in Fig. 8. The three-pole low-pass filter leads to 270° of phase lag deep in the stopband.

The input-referred noise of the two-stage amplifier was measured by grounding the inputs, measuring the output noise using a sensitive low-noise preamplifier (Stanford Research Systems SR560) connected to an oscilloscope and low-frequency spectrum analyzer (Stanford Research Systems SR770), and dividing by the amplifier gain of 200 V/V. Fig. 9 shows the input-referred noise of an amplifier with f_H set to 10 kHz; Fig. 10 shows the input-referred noise for the same amplifer set to f_H = 100 Hz. In both cases, the input-referred noise is 2 μV_{rms} since the reduction in bandwidth is balanced by the increase in thermal noise due to lower bias currents.

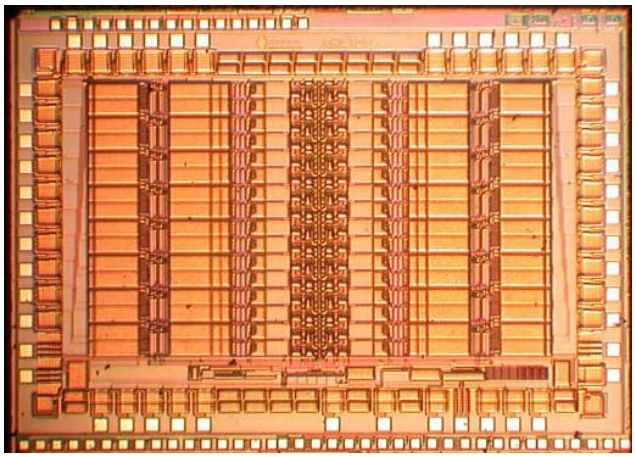

Fig. 6. Die photo of the 16-channel bioamplifier integrated circuit. The chip measures 4.3 × 3.1 mm^2.

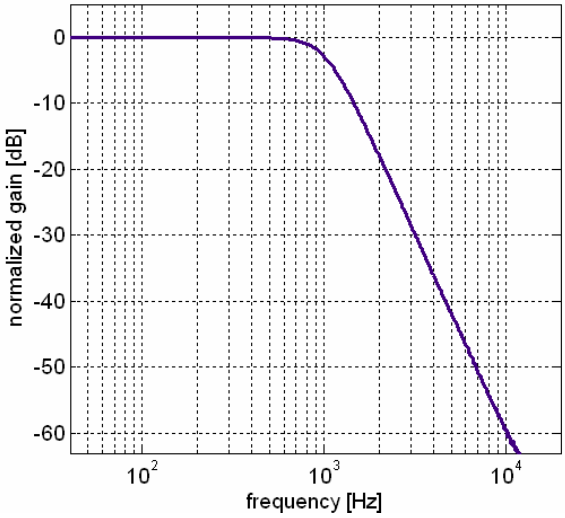

Fig. 7. Measured normalized gain vs. frequency for f_H = 1 kHz.

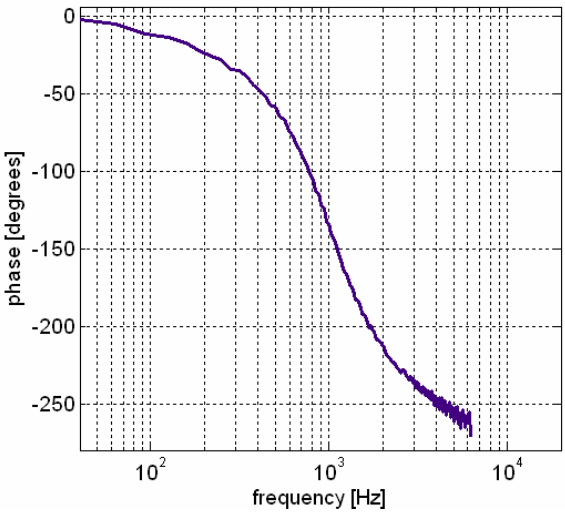

Fig. 8. Measured phase lag vs. frequency for f_H = 1 kHz.

Fig. 11 shows the measured input-referred noise spectra for amplifiers with f_H set to 10 Hz, 100 Hz, 1 kHz, and 10 kHz. The higher thermal noise levels with lower bandwidths are evident in the data. Notice that due to the relatively high thermal noise levels (and the use of large gate area pMOS devices in the input differential pair) $1/f$ noise only dominates at frequencies less than approximately $0.1f_H$. Thus, flicker noise does not dominate the total rms input-referred noise, which stays nearly constant at 2 μV_{rms} across all values of f_H.

We measured the common-mode rejection ratio (CMRR) for 48 amplifiers across three chips, testing at frequencies of 60 Hz and 1 kHz. At both frequencies, the average CMRR was 84 dB. Observed CMRR values ranged from 71 dB to 101 dB. Power-supply rejection ratio (PSRR) was also measured across these 48 amplifiers at 60 Hz and 1 kHz. At both frequencies, the average PSRR was 75 dB. Observed PSRR values ranged from 66 dB to 92 dB. Input-referred voltage offset was measured across 96 amplifiers on six chips. Input-referred offset was symmetrically distributed about zero with a standard deviation of 170 µV. The largest observed offsets were ±430 µV.

B. Biopotential Measurements

After benchtop characterization was completed, we used the RHA1016 integrated circuit to amplify real biopotentials obtained using commercially available electrodes. We used adhesive Ag/AgCl electrodes to obtain human ECG and EMG signals (see Figs. 12 and 13). In both cases, the differential recording electrodes were positioned approximately 5 cm apart, with the amplifier ground connected to an Ag/AgCl electrode on the elbow. For ECG recordings, the amplifier was configured to have a bandwidth of 100 Hz; for EMG recordings, the bandwidth was set to 1 kHz.

Human EEG recordings were obtained using Ag/AgCl electrodes filled with electrolyte gel on an elastic cap, with amplifier ground connected to the left earlobe. Fig. 14 shows 10-Hz, 60-μV_{pp} alpha waves recorded from the occipital region in the back of the head (over primary visual cortex) from standard electrode positions O_1-O_2 [10] with the amplifier bandwidth set to 50 Hz. The subject's eyes were closed initially, then opened at $t = 0$, suppressing the alpha waves. (Alpha waves in the 10-Hz range commonly appear in the occipital region when the eyes are closed.) Fig. 15 shows a human EEG signal recorded from frontal region F_{p1}-F_3 on the forehead. Two eye-blink artifacts (commonly observed in this region of the head) are visible.

Neural recordings were obtained using a MEMS 100-microelectrode array (Cyberkinetics, Inc., Foxborough, MA) implanted in the motor cortex of a cat. The recordings were performed approximately three months after implantation. A platinum wire implanted near the array was used for the reference signal, and the amplifier ground was connected to a small metal pedestal on the cat's head that served as a connector to the electrode array and reference wire. The cat was awake and comfortably resting during the measurements.

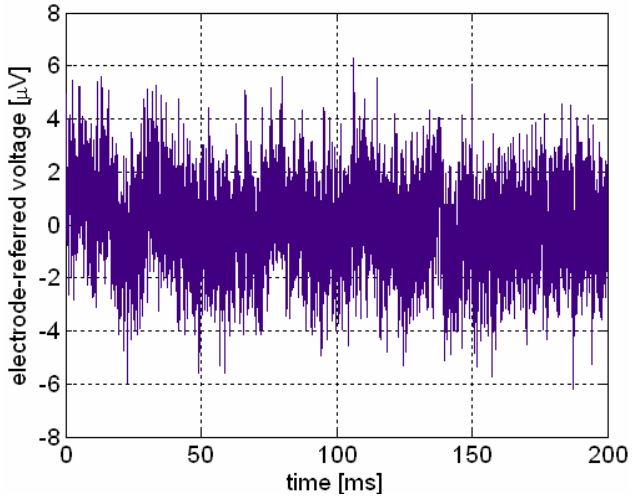

Fig. 9. Measured input-referred noise for f_H = 10 kHz.

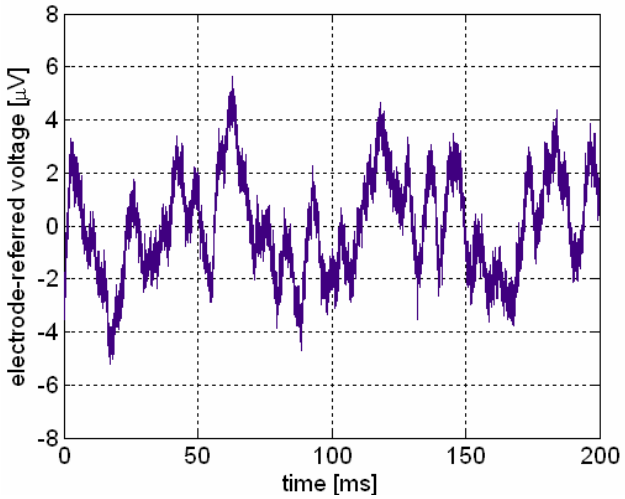

Fig. 10. Measured input-referred noise for f_H = 100 Hz.

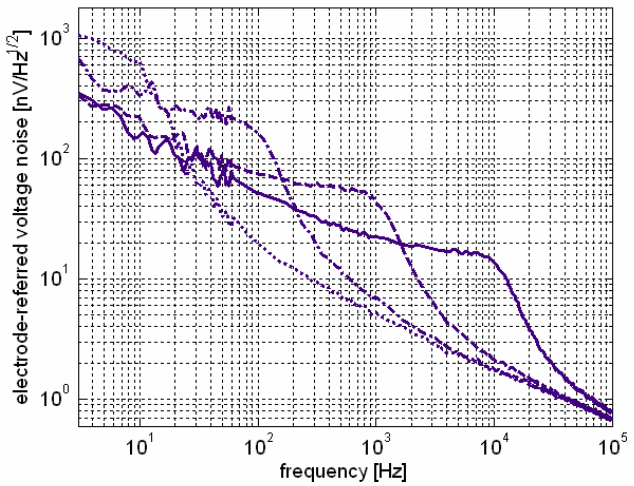

Fig. 11. Input-referred noise spectra for f_H = 10 Hz (dot), f_H = 100 Hz (dash-dot), f_H = 1 kHz (dash), and f_H = 10 kHz (solid).

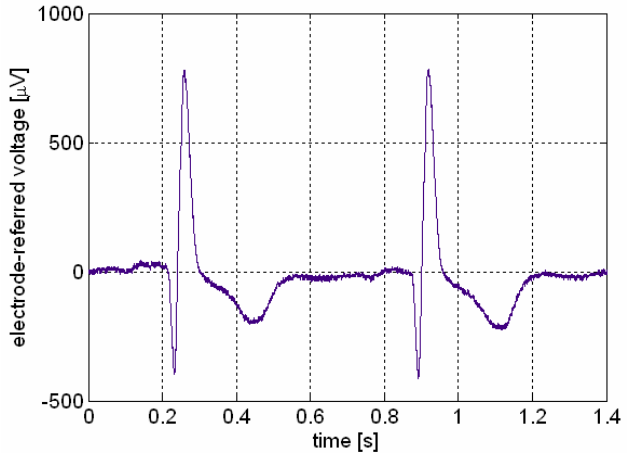

Fig. 12. ECG signal recorded with Ag/AgCl electrodes on the chest (f_H = 100 Hz).

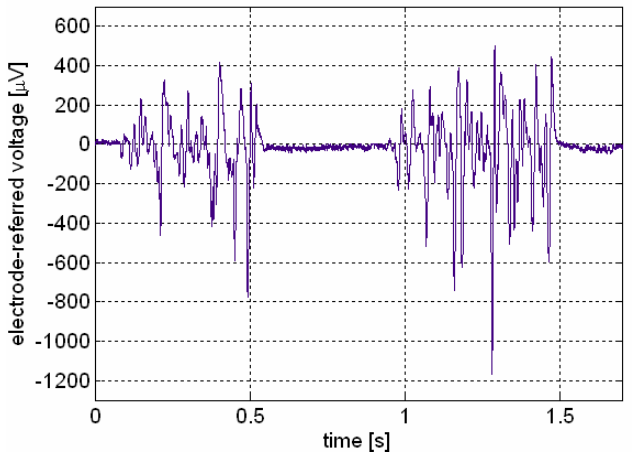

Fig. 13. EMG signal recorded with Ag/AgCl electrodes over bicep during two brief muscle contractions (f_H = 1 kHz).

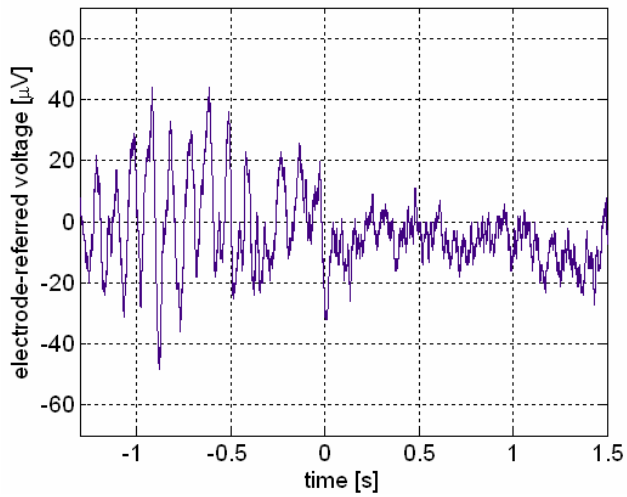

Fig. 14. EEG signal with 10-Hz alpha waves recorded from occipital region O_1-O_2 (f_H = 50 Hz). Subject's eyes were closed initially, then opened at t = 0, suppressing the alpha waves.

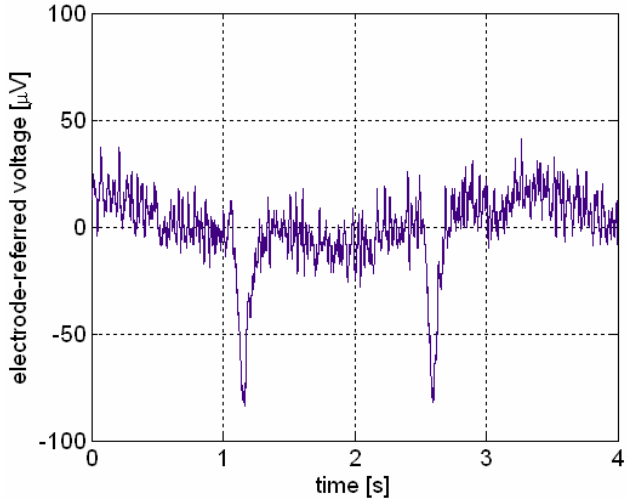

Fig. 15. EEG signal recorded from frontal region Fp_1-F_3 on the forehead (f_H = 50 Hz). Two eye-blink artifacts (commonly observed in this region of the head) are visible.

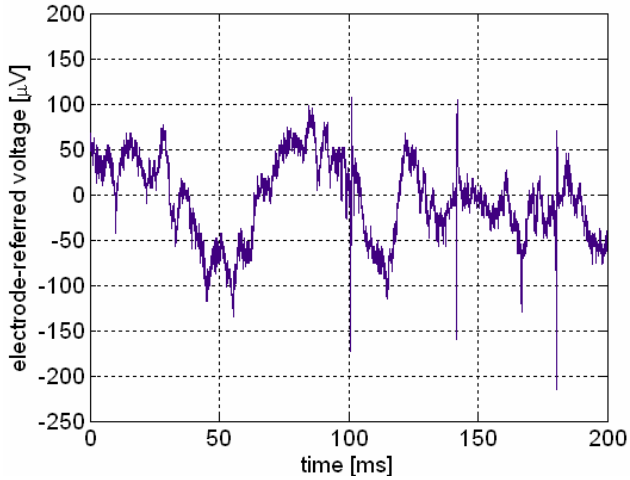

Fig. 16. Neural recording from motor cortex of cat with MEMS electrode array showing both spikes and LFPs (f_H = 5 kHz).

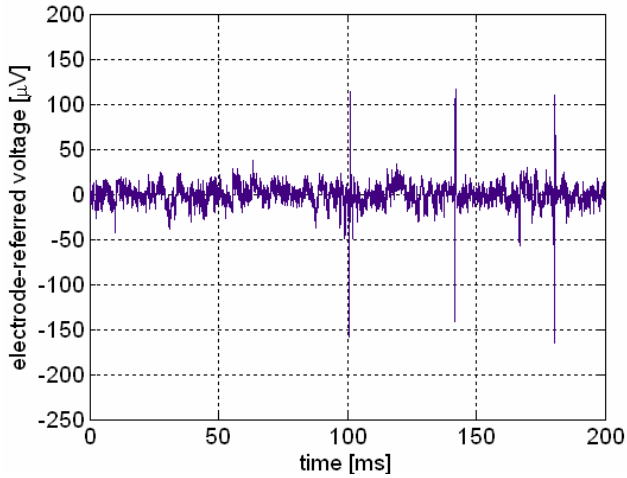

Fig. 17. Data from Fig. 16 after a 300-Hz one-pole high-pass filter was applied in software to remove LFPs and preserve spikes.

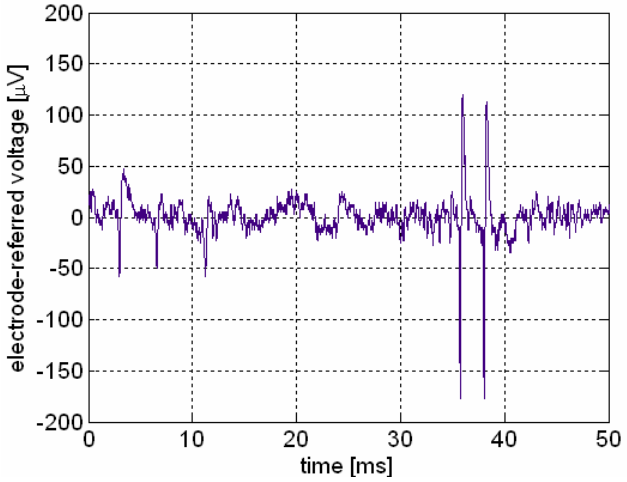

Fig. 18. Large and small spikes observed in motor cortex of cat. (A one-pole high-pass filter at 300 Hz was applied to the signal.)

Fig. 16 shows a 200-ms segment of spontaneous neural activity recorded using an amplifier with f_H = 5 kHz. Both low-frequency local field potentials (LFPs) and high-frequency neural spikes are observed. This data was digitally high-pass filtered to attenuate signals below 300 Hz (see Fig. 17). This eliminates the LFP signals while preserving the spikes. Fig. 18 shows another neural waveform that was high-pass filtered at 300 Hz. Here, both large- and small-amplitude spikes (presumably originating from two distinct neurons) can be observed. In Fig. 19, several neural spikes are aligned based on the time they crossed a user-defined threshold. This plot demonstrates that 2-3 distinct neurons with consistent waveforms are being observed.

Fig. 20 demonstrates the ability of the amplifier to observe trends in the low-frequency LFP signals over this seven-second span. Around t = 2.5 s, strong beta-wave activity in the 10-15 Hz range appears. This activity can be seen clearly in a spectrogram of the data presented in Fig. 21. Although it is difficult to see in Fig. 20 due to the extended time scale, this data contains both spikes and LFPs that are easily separated with simple digital post-processing.

Finally, to demonstrate the ability of the amplifier to record very-low-frequency signals, we recorded an action potential from the Venus flytrap plant (*Dionaea muscipula*) using Ag/AgCl electrodes placed on either side of a trap, with amplifier ground tied to the soil (see Fig. 22). The amplifier was configured to have a bandwidth of 50 Hz. When a trigger hair inside the trap was bent, an action potential lasting several seconds was produced [1]. (This isolated stimulus did not cause closure of the trap, so no movement artifacts are present in the data.)

V. Conclusion

The measured characteristics of the integrated biopotential amplifier chip are summarized in Table I. The total power dissipation of the chip depends on the desired amplifier

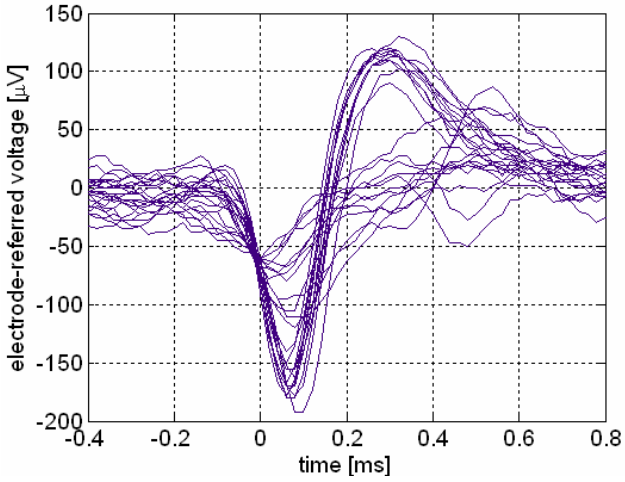

Fig. 19. Several time-aligned spikes from motor cortex of cat.

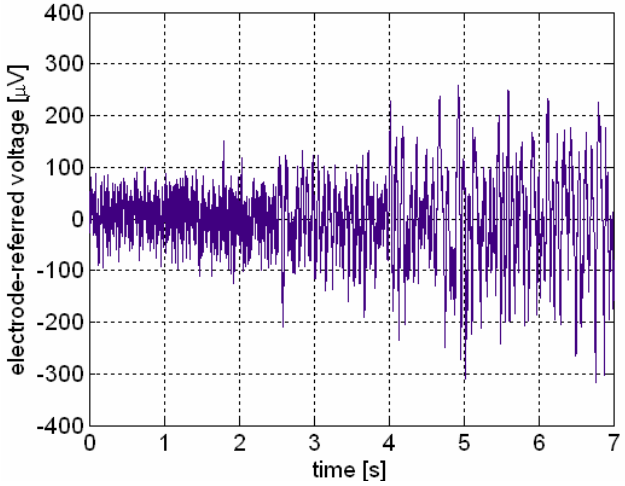

Fig. 20. Seven-second neural recording from motor cortex of cat showing onset of 10-15 Hz beta activity in the local field potential.

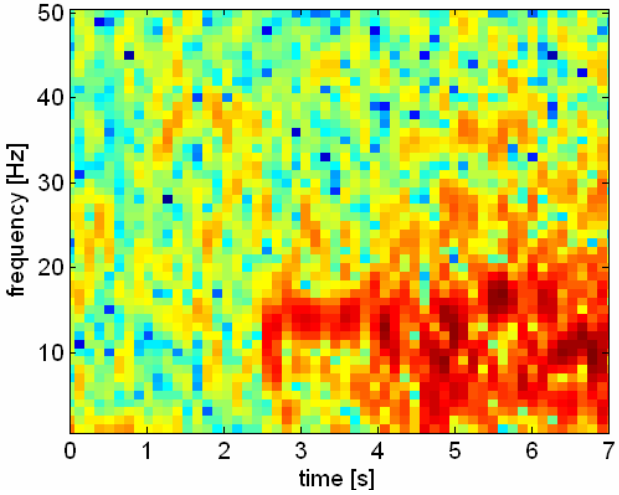

Fig. 21. Spectrogram of neural data from Fig. 20.

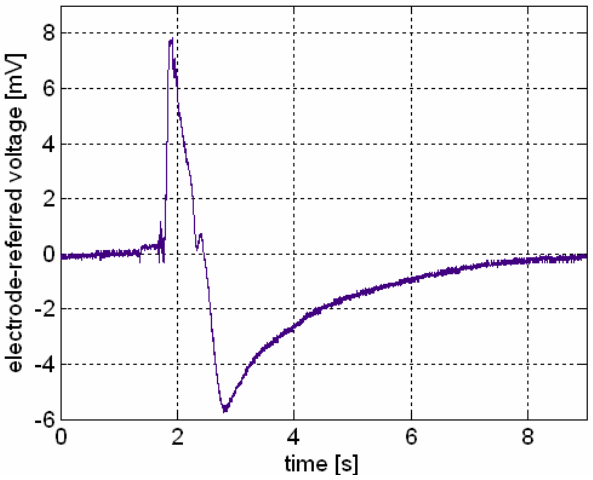

Fig. 22. Action potential measured from Venus flytrap (*Dionaea muscipula*) during bending of trigger hair (f_H = 50 Hz).

bandwidth. For f_H = 10 kHz, the chip consumes 41 mW. For bandwidths of 1 kHz or less the chip consumes 28 mW, as total power dissipation is dominated by the fast buffers in the analog MUX that provide a settling time of less than 1 µs. At a bandwidth of 1 kHz, the power consumption of a single two-stage amplifier shown in Fig. 4 is 460 µW.

The amplifier presented here is designed to pass signals from less than 0.1 Hz up to a user-specified high-frequency cutoff. In addition to attenuating high-frequency noise, the 3rd-order lowpass filter at f_H acts as a built-in anti-aliasing filter and permits low-frequency signals such as EEGs or ECGs to be digitized at a slower rate than higher-frequency signals such as neural spikes. For highly parallel recording systems with large numbers of channels, it makes sense to limit the sampling frequency to minimize the rate at which data must be stored or transmitted. In wideband recordings, undesired low-frequency signals (e.g., LFPs) can be easily filtered out digitally after digitization.

Although the bandwidth of this amplifier is variable, the gain is fixed at 200 V/V. A variable-gain architecture was considered, but modern high-quality analog-to-digital converters (ADCs) diminish the need for this degree of control. To illustrate this claim, consider that the amplifier input-referred noise of 2 μV_{rms} produces a 400 μV_{rms} noise signal at the output. A 16-bit ADC operating across 5 V can resolve steps of 76µV, so increasing the gain beyond 200 accomplishes little at the system level.

This chip might benefit somewhat from fabrication in a smaller process, though much of the silicon area is consumed by linear capacitors (~1 fF/µm^2) which do not scale greatly in deep submicron processes. Alternately, die area could be reduced by trading off increased input-referred noise levels for decreased capacitor values [6] or lower-order filtering at f_H.

TABLE I
MEASURED AMPLIFIER PERFORMANCE

Parameter	Measured Value	Comments
Midband differential gain (A_M)	46.0 dB 200 V/V	linear up to ±5 mV ac amplitude input
Low-frequency 3-dB cutoff (f_L)	< 0.05 Hz	1-pole roll-off below f_L
High-frequency 3-dB cutoff (f_H)	tunable from 10 Hz to 10 kHz	3rd-order Butterworth filter roll-of above f_H
Temperature coefficient of f_H	+0.4 %/°C	
CMRR	71 dB – 101 dB mean CMRR: 84 dB	measured at 60 Hz and 1 kHz with f_H = 10 kHz
PSRR	66 dB – 92 dB mean PSRR: 75 dB	measured at 60 Hz and 1 kHz with f_H = 10 kHz
Crosstalk	< –90 dB (0.05 Hz to 10 kHz)	measured between adjacent amplifiers
Input offset voltage	< ±0.6 mV	Input offset varies –1.0 µV/°C with temp.
Input bias current	typ. 3 pA	current due to ESD protection structures
Input-referred noise	2 μV_{rms}	
Total harmonic distortion	2 mVpp input: 0.1% 10 mVpp input: <1%	f = 1 kHz, f_H = 10 kHz
Dynamic range	65 dB	
MUX settling time	< 1.0 µs	allows sampling at 30 kHz per channel
Total 16-amplifier chip power dissipation	28 mW (f_H = 1 kHz) 41 mW (f_H = 10kHz)	includes high-speed analog MUX

ACKNOWLEDGMENTS

Chip fabrication and testing was funded by Intan Technologies, LLC (Salt Lake City, UT). The author thanks Bradley Greger at the University of Utah Bioengineering Department for collaborations yielding the neural data presented in this paper.

REFERENCES

[1] O. Stuhlman, Jr. and E.B. Darden, "The action potentials obtained from Venus's-flytrap," *Science,* vol. 111, pp. 491-492, 1950.

[2] E.R. Kandel, J.H. Schwartz, and T.M. Jessell, *Principles of Neural Science,* 4th ed. Boston, MA: McGraw-Hill, 2000.

[3] C.D. Ferris, *Introduction to Bioinstrumentation.* Clifton, NJ: Humana, 1978.

[4] A.C. Hoogerwerf and K.D. Wise, "A three-dimensional microelectrode array for chronic neural recording," *IEEE Trans. Biomed. Eng.,* vol. 41, pp. 1136-1146, Dec. 1994.

[5] C.T. Nordhausen, E.M. Maynard, and R.A. Normann, "Single unit recording capabilities of a 100-microelectrode array," *Brain Res.,* vol. 726, pp. 129-140, 1996.

[6] R.R. Harrison and C. Charles, "A low-power low-noise CMOS amplifier for neural recording applications," *IEEE J. Solid-State Cir.,* vol. 38, pp. 958-965, June 2003.

[7] C.C. Enz, F. Krummenacher, and E.A. Vittoz, "An analytical MOS transistor model valid in all regions of operation and dedicated to low-voltage and low-current applications," *Analog Integrat. Circuits Signal Process.,* vol. 8, pp. 83-114, 1995.

[8] Y. Tsividis, *Operation and Modeling of the MOS Transistor,* 2nd ed. Boston, MA: McGraw-Hill, 1998.

[9] D.A. Johns and K. Martin, *Analog Integrated Circuit Design.* New York, NY: John Wiley & Sons, 1997.

[10] E. Niedermeyer and F. Lopes da Silva, *Electroencephalography,* 2nd ed. Baltimore, MD: Urban & Schwarzenberg, 1987.